An Adaptive Strategy Based on Repetitive Predictive Control for Improving Adaptability of *LCL*-Type Grid-Connected Inverters Under Weak Grid

Mingming Li, Huafeng Xiao, *Senior Member, IEEE*, and Ming Cheng, *Fellow, IEEE*

***Abstract*—For current-controlled grid-connected inverters with *LCL* filter, the essence of grid voltage full feedback is to improve the output impedance of grid-connected inverters to infinity, which can eliminate the influences of grid voltage distortion and the non-negligible grid impedance. However, existing full feedforward strategies are complex and control delay cannot be compensated precisely, which leads to the instability of system when the full feedforward of the voltage at the point of common coupling under the weak grid is adopted. This article first proposes a simplified full feedforward strategy based on grid-side inductor volt-age differential feedback active damping (GIVD-AD). Second, repetitive prediction (RP) is used to compensate for the control delay. Then, a virtual impedance branch is added and an adaptive algorithm for modifying virtual impedance based on the difference between predicted grid voltages by Newton interpolation prediction (NIP) and RP is proposed. With the proposed method, grid-connected inverters can work stably when grid impedance changes suddenly and exhibit strong rejection ability against grid-voltage harmonics. Finally, simulative and experimental results from a 3-kW single-phase grid-connected inverter are provided to prove the effectiveness of the proposed strategy.**

***Index Terms*—Adaptive control, control delay, grid voltage full feedforward, weak grid.**

I. Introduction

RECENTLY, distributed power generation system (DPGS) technique has become a considerable means to deal with the abuse of fossil fuels and the increasing seriousness of environmental pollution. However, as the proportion of DPGS in the grid gradually increases, its impact on the grid is becoming more and more non-negligible [1]. Long-distance transmission lines, countless low-voltage isolation transformers, a large number of distributed generation devices, and various nonlinear devices connected to point of common coupling (PCC), resulting in a nonideal grid that can be equated to a harmonic-rich voltage source in series with inductive impedances [2]. Compared to the stiff grid, the weak grid has two disadvantages: First, the grid voltage at PCC usually contains varieties of background harmonics; second, the grid impedance is non-negligible and varies over a wide range. As a consequence, the grid harmonics distort the injected grid-in current and the grid impedance challenges the inverter system stability [3].

Generally, there are two kinds of methods to suppress the grid current harmonics caused by PCC voltage distortion. One is employing multiple resonant compensators to increase output impedance at the harmonic frequencies for selective harmonic elimination [4]. The other one is using PCC voltage feedforward, including proportional and full feedforward means [5]–[7], which equivalently emulates a parallel admittance term to increase the output impedance of the inverter greatly. In summary, the essence of these two types of methods is to increase the output impedance to improve the anti-interference capability of grid-connected inverters [8]. All these methods show a satisfactory performance under the stiff grid. However, the grid impedance in a weak grid would reduce the cut-off frequency of the grid-connected system. When the cut-off frequency is less than the resonant frequency of the resonant compensators, the grid-connected system will be instable [9]. Likewise, the feedforward scheme may also lead to system instability due to the control delay [10].

In order to boost the output impedance of grid-connected inverters, a more robust controller can be used to solve the problem of system instability due to the grid impedance, such as robust controllers [11]. However, these controllers are usually nonlinear, and the design methods are complex and less universal. At the same time, the design difficulty will be further increased if the background harmonic suppression of the grid is taken into account [12]. In addition, it is also possible to measure the grid impedance online and apply corresponding control strategies to offset the influence on the grid-connected system. Generally, this type of method tends to reduce the quality of the grid-in current and increase the computational burden [13]–[15]. However, grid impedance estimation based on variations of the output power in [16]–[18] are proved that they not only can measure the grid impedance accurately but also overcome the disadvantages, such as power quality issues and complex calculation.

According to the aforementioned description, both the injected current quality and the stability are significant to grid-connected inverters under weak grid conditions. Thus, this study firstly deduces a simplified grid voltage full feedforward strategy based on the grid-side inductor voltage differential

Manuscript received May 18, 2021; revised July 20, 2021; accepted August 25, 2021. Date of publication September 1, 2021; date of current version November 30, 2021. Recommended for publication by Associate Editor M. Liserre. *(Corresponding author: Huafeng Xiao.)*

The authors are with the Department of Electrical Engineering, Southeast University, Nanjing 210096, China (e-mail: mmlsvg@163.com; xiaohf@seu.edu.cn; mcheng@seu.edu.cn).

Color versions of one or more figures in this article are available at https://doi.org/10.1109/TPEL.2021.3108878.

Digital Object Identifier 10.1109/TPEL.2021.3108878

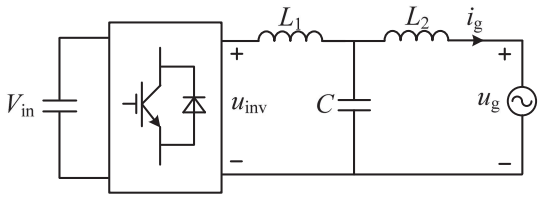

Fig. 1. *LCL*-filtered grid-connected inverter.

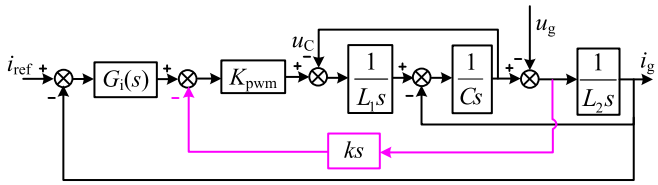

Fig. 2. Control block diagram of grid-connected inverter.

feedback active damping (GIVD-AD) and points out that grid voltage full feedforward can completely eliminate the influence of distorted voltage on the injected current in theory. Then it proves that the grid voltage full feedforward under weak grid can lead to system instability because of the delay and the grid impedance. Therefore, a repetitive prediction (RP) is employed to compensate for the delay. However, it proves that the delay compensation method cannot guarantee the system stability due to errors of compensation. Thus, a virtual impedance branch is added to solve the problem, and considering that the grid impedance may change under different operating conditions, an adaptive strategy is proposed to automatically adjust the virtual impedance based on the difference between the predicted grid voltages by NIP and RP, which can stabilize the grid-connected system and enhance the robustness.

Compared to the existing grid voltage full feedforward methods, the proposed full feedforward strategy reduces the number of full feedforward branches. Meanwhile, because the reduced feedforward branch contains a differential module, the amplification of harmonics in the grid voltage can be avoided. Therefore, the proposed full feedforward strategy helps to reduce the system complexity and improve the quality of the grid-in current. Besides, the adaptive algorithm for modifying virtual impedance aims at the optimal grid-in current, and it is based on solving the digital control delay, which helps to reduce the complexity of the control system.

The rest of this article is organized as follows. In Section II, the simplified form of grid voltage full feedforward based on GIVD-AD is derived. Section III analyzes the influence of delay and provides a solution. The virtual impedance is added to solve the problem of system instability, and the principle of automatically determining the optimal virtual impedance is presented in Section IV. Waveforms in Section V validate the theoretical analysis and the effectiveness of the proposed strategy. Finally Section VI concludes this article.

II. Grid Voltage Full Feedforward Based on GVID-AD

Fig. 1 shows a generic structure of the *LCL*-filtered grid-connected inverter, it consists of an inverter-side inductor L_1, a filter capacitor C, and a grid-side inductor L_2. $V_{\rm in}$ is the input dc voltage, $u_{\rm inv}$ is the output voltage of inverter bridge, $i_{\rm g}$ is the grid current, and $u_{\rm g}$ is the grid voltage.

A. Grid Voltage Full Feedforward Strategy Based on GVID-AD

Fig. 2 shows a control block diagram of the grid-connected system with GIVD-AD. In Fig. 2, $G_{\rm i}(s)$ is the current regulator, $K_{\rm pwm}$ is the transfer function of the inverter bridge and k is the feedback coefficient of AD loop.

By using GIVD-AD, it can simplify the grid voltage full feedforward compared to the conventional filter capacitor current proportional-feedback AD. The proof process is as follows.

According to Fig. 2, the expression of $i_{\rm g}$ can be derived as (1), shown at the bottom of this page, which indicates that $i_{\rm g}$ is related to the reference current $i_{\rm ref}$ and $u_{\rm g}$. With the use of the signal flow graph method in [19], Fig. 2 can be transformed into Fig. 3(a), where the expression of $G_{\rm x1}(s)$ can be expressed as

$$G_{\rm x1}(s) = \frac{K_{\rm pwm}G_{\rm i}(s)}{s^2L_1C+1}. \tag{2}$$

Note that the expression of $G_{\rm x1}(s)$ includes the current regulator $G_{\rm i}(s)$. In order to simplify, it can move the feedforward node from the input of $G_{\rm i}(s)$ to the output of it, where the feedforward component contributes to the modulation of the duty cycle, and the $u_{\rm g}$ full feedforward branch has been changed into $G_{\rm i}(s)/G_{\rm x1}(s)$. Then, substituting the expressions of $G_{\rm i}(s)$ and $G_{\rm x1}(s)$, (3) can be derived

$$\frac{G_{\rm i}(s)}{G_{\rm x1}(s)} = \frac{s^2L_1C}{K_{\rm pwm}} + \frac{1}{K_{\rm pwm}}. \tag{3}$$

Therefore, Fig. 3(a) can be transformed into Fig. 3(b). Obviously, with adopting GIVD-AD, the $u_{\rm g}$ full feedforward contains only two branches. Compared to [19], the differential branch is eliminated. Because the differential branch can amplify grid background harmonics, the full feedforward based on GVID-AD minimizes the influence of distorted $u_{\rm g}$. Therefore, the proposed full feedforward strategy based on GVID-AD is more practical in the actual situation.

B. Relation Between Grid Voltage Full Feedforward and Inverter Output Impedance

From the above analysis, $u_{\rm g}$ full feedforward can be equivalent to connecting a negative impedance $Z_{\rm o}'(s)$ in parallel with

$$i_{\rm g} = \frac{K_{\rm pwm}G_{\rm i}(s)}{s^3L_1L_2C+s^2K_{\rm pwm}kCL_2+s(L_1+L_2)+K_{\rm pwm}G_{\rm i}(s)}i_{\rm ref} - \frac{s^2L_1C+1}{s^3L_1L_2C+s^2K_{\rm pwm}kCL_2+s(L_1+L_2)+K_{\rm pwm}G_{\rm i}(s)}u_{\rm g} \tag{1}$$

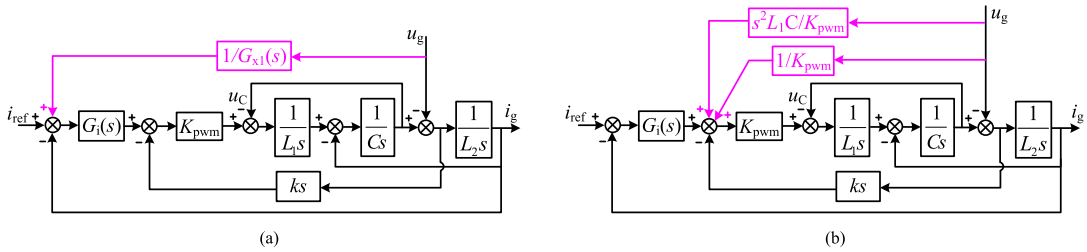

Fig. 3. Control block diagram of u_g full feedforward with GIVD-AD. (a) Equivalent transformation I. (b) Full feedforward control block diagram.

inverter output impedance, which can be expressed as follows:

$$Z_o'(s) = \frac{s^2 L_1 C+1}{s^3 L_1 L_2 C+s^2 K_{PWM} k L_2 C+s(L_1+L_2)+K_{PWM} G_i(s)}. \quad (4)$$

A schematic diagram of the grid-connected system is given in Fig. 4, where $i_s(s)$ is the Norton equivalent current source and $Z_o(s)$ represents output impedance of the grid-connected inverter seen from PCC, including the impedance of the filter.

After adding $Z_O'(s)$, the output impedance of grid-connected inverter can be expressed as

$$Z_{op}(s) = \frac{Z_o(s) Z_o'(s)}{Z_o(s) + Z_o'(s)}. \quad (5)$$

Then, the expression of i_g(s) can be derived as

$$i_g(s) = i_s(s) - \frac{u_g(s)}{Z_{op}(s)}. \quad (6)$$

When $Z_O'(s)$ and $Z_o(s)$ are equal in magnitude and opposite in sign, $Z_{op}(s)$ becomes infinite. According to (6), the influence of u_g is negligible in this situation, and the same effect can be achieved by full feedforward. The above-mentioned analysis shows that full feedforward is essentially raising the output impedance of the inverter to infinity to eliminate the influence of u_g.

In a weak grid, the grid impedance $Z_g(s)$ cannot be ignored, and in this situation, the injected grid current $i_g(s)$ can be derived as

$$i_g(s) = \frac{Z_{op}(s)}{Z_{op}(s) + Z_g(s)} i_s(s) - \frac{u_g(s)}{Z_{op}(s) + Z_g(s)}. \quad (7)$$

When $u_g(s)$ is fully feedforward, $Z_{op}(s)$ tends to infinity based on the above analysis. According to (7), i_g is approximately equal to the Norton equivalent current $i_s(s)$, and the influence of u_g on i_g is negligible. This can prove that even when $Z_g(s)$ is not negligible, the full feedforward of $u_g(s)$ can keep the system stable and i_g is not affected by u_g anymore.

However, because of other nonideal factors such as control delay and it only measures the voltage u_{PCC} only, the full feedforward of u_{PCC} is not able to eliminate the influence of the distorted u_g and it might even lead to grid-connected systems instability in the week grid.

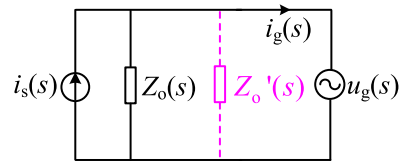

Fig. 4. Equivalent circuit of grid-connected system.

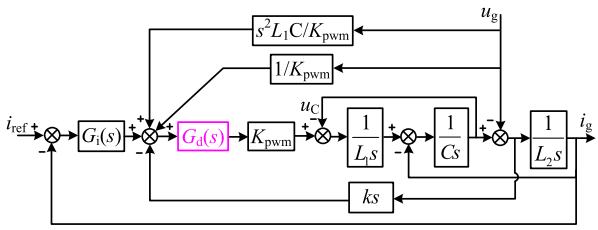

Fig. 5. Control block diagram with delay.

III. Influence of Control Delay on Grid Voltage Full Feedforward and the Solution

A. Influence of Control Delay on Output Impedance of Grid-Connected Inverters

When considering control delay, grid-connected systems control block diagram can be drawn as Fig. 5.

$G_d(s)$ represents control delay, which usually includes the computation delay, the pulsewidth modulation (PWM) delay, and the sampler.

According to Fig. 5, the output impedance of grid-connected inverters can be calculated, respectively, when the proportional and full feedforward are employed, as shown at the bottom of this page.

$Z_{OPF}(s)$ represents the out impedance of grid-connected inverters with the use of proportional feedforward and $Z_{OFF}(s)$ represents the out impedance with the use of full feedforward.

$$Z_{OPF}(s) = \frac{s^3 L_1 L_2 C + s^2 K_{PWM} k C L_2 G_d(s) + s(L_1+L_2) + K_{PWM} G_i(s) G_d(s)}{s^2 L_1 C + 1 - G_d(s)} \quad (8)$$

$$Z_{OFF}(s) = \frac{s^3 L_1 L_2 C + s^2 K_{PWM} k C L_2 G_d(s) + s(L_1+L_2) + K_{PWM} G_i(s) G_d(s)}{(s^2 L_1 C + 1)(1 - G_d(s))} \quad (9)$$

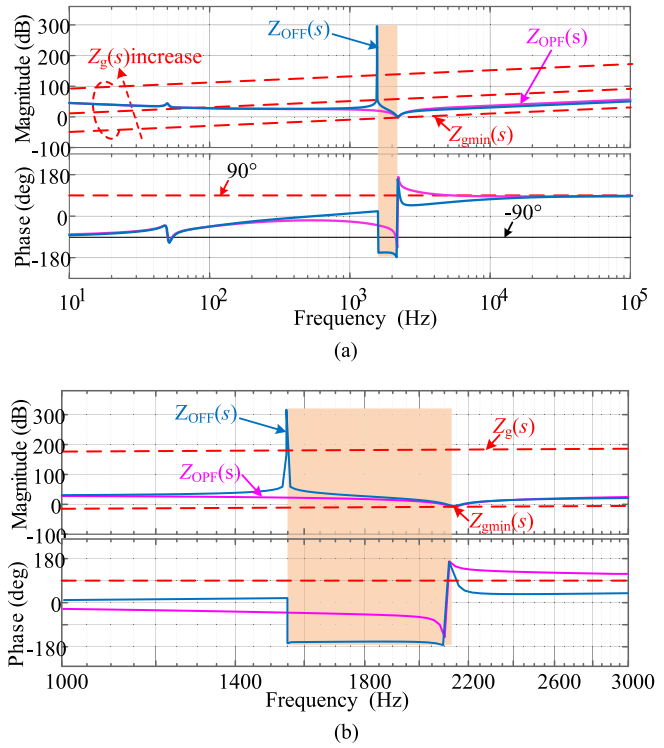

Fig. 6. Bode plots of grid impedance and output impedance of the inverter. (a) Overall curves. (b) Detail curves.

Because of the delay, the output impedance is no longer tending to infinity when full feedforward strategy is adopted. Therefore, the influence of a weak grid on grid-connected systems needs to be re-evaluated.

To guarantee stability, grid-connected inverters must satisfy that the ration between $Z_g(s)$ and the output impedance $Z_o(s)$ satisfies the Nyquist criterion. The impedance ratio $Z_g(s)/Z_o(s)$ satisfies the Nyquist criterion, i.e., there is no intersection between the magnitude-frequency curves of $Z_g(s)$ and $Z_o(s)$, or if intersection occurs, the phase margin (PM) at the intersection frequency is positive [9]. Here, the PM is expressed as

$$\mathrm{PM} = 180^\circ - (\angle Z_g - \angle Z_o) > 0. \tag{10}$$

Since resistor offers some degree of damping and helps to stabilize grid-connected systems, a pure inductor is considered here to draw the worst case. At this situation, it can be deduced that the phase of $Z_o(s)$ at the intersection frequency must be above -90° to ensure PM>0.

Fig. 6 gives the Bode plots of the inverter output impedance with different feedforward strategies. According to the above-mentioned analysis, in the area where the angle of the inverter output impedance is less than -90°, i.e., the shaded part in Fig. 6, the system will be unstable if there is an intersection between the amplitude–frequency curve of the inverter output impedance and the grid impedance. Since the amplitude–frequency curve of $Z_{OFF}(s)$ has a large peak, it can be concluded that if the grid impedance exceeds $Z_{gmin}(s)$ in Fig. 6, then its amplitude–frequency curve will intersect with the amplitude–frequency curve of $Z_{OFF}(s)$ in the shaded area, and the system will be destabilized.

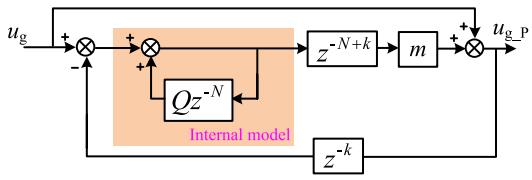

Fig. 7. Control block diagram of RP.

In contrast, if the grid voltage is proportional feedforward, the $Z_{OPF}(s)$ less than -90° contains a very small area. This proves that the stability margin of system with grid voltage proportional feedforward is greater than full feedforward. However, it can be seen from Fig. 6(a) that as the grid impedance increases, the angle of $Z_{OPF}(s)$ gets closer to -90° where its magnitude–frequency curve intersects with the grid impedance, which indicates that the stability margin of the system is also decreasing. Therefore, whether grid voltage is proportional or full feedforward, the system will be destabilized when the grid impedance increases to a certain level.

B. Solution Against the Delay

Based on the above analysis, the delay leads to the instability of grid-connected systems. The solutions against control delay, without changing the switching frequency, fall into two categories. One of them is shifting the sampling instant toward the PWM reference update instant, and the computation delay can be reduced [20]–[23]. However, this kind of method has the problem of frequency aliasing, and the delay caused by PWM and sampling circuit cannot be eliminated. Another adopts the phase compensator, such as phase-lead compensator and interpolation forecasting method, but they amplify the harmonic amplitude and affect the power quality.

Considering the fundamental wave and harmonics, they have the following two characteristics: one is that the signals have repeatability; the other one is that the frequencies of harmonics are integer multiple of the fundamental wave.

The RP based on the internal mode principle can provide high gain at the fundamental frequency and its integer multiples [24], [25]. Alhough there are abundant background harmonics in the grid, the RP based on internal model can theoretically predict the grid voltage without error, so it will not amplify the amplitudes of higher harmonics and has excellent steady-state tracking performance. In addition, because the RP was only used for prediction and did not participate in the control of grid-in current, the shortcomings of poor dynamic characteristics of the internal model controller can be avoided.

Taking u_g prediction as an example, the control block diagram of RP is shown in Fig. 7, where Q is a low-pass filter or a constant less than 1, N represents the number of switching cycles T_s in a grid cycle, k represents the number of T_s to be predicted, and m represents the gain coefficient less than 1 generally.

Referencing the design method of RPs parameters in [25], $Q = 0.98$ and $M = 0.96$ are selected. The switching frequency

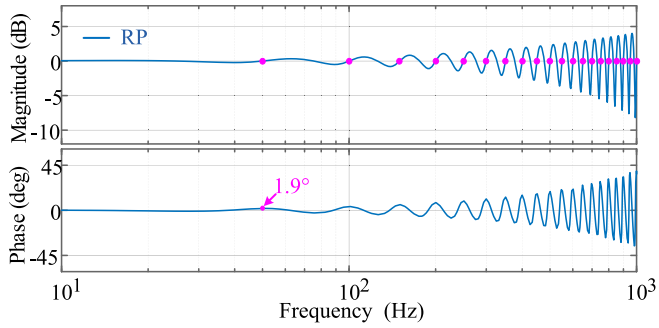

Fig. 8. Bode plot of RP.

is 18 kHz, so $N = 360$. Considering the delay of the sampling circuit, $k = 2$ is selected.

According to Fig. 7, the transfer function of RP can be deduced as

$$G_{RP} = \frac{1 - Qz^{-N} + mz^{-N+k}}{1 - Qz^{-N} + mz^{-N}}. \tag{11}$$

The Bode plot of (11) is drawn, as shown in Fig. 8. As can be seen from Fig. 8, the amplitude gains of fundamental and harmonic are close to 0 dB, indicating that RP hardly amplifies the amplitudes of fundamental and harmonics. The phase gain of the fundamental is 1.9°, and the error is close to 5%, mainly because the values of Q and M are less than 1, which sacrifices the no-static error characteristic of the ideal internal mode to increase the robustness of system. But compared with the conventional prediction methods, RP avoids the amplification of harmonics.

NIP is essentially a polynomial interpolation method, which is an improvement of the conventional Lagrangian interpolation method [26]. Compared with the Lagrangian interpolation method, it not only overcomes the disadvantage that the whole calculation must be restarted when adding a node, but also saves the number of multiplication and division operations. In addition, the predicted polynomial can be improved when using NIP to forecast grid voltage because the frequency of the update of sampled grid voltage value is fixed. As an example, NIP is used to predict the grid voltage for N switching cycles, and it can be expressed as

$$\begin{aligned} u_{\text{out}}(k) = {} & u_{\text{g}}(k) + k_1(u_{\text{g}}(k) - u_{\text{g}}(k-1)) \\ & + k_2(u_{\text{g}}(k-1) - u_{\text{g}}(k-2)) \end{aligned} \tag{12}$$

where $u_{\text{out}}(k)$ represents the grid voltage after predicting N switching cycles, $u_{\text{g}}(k)$ represents the grid voltage sampled in the current switching interruption, $u_{\text{g}}(k\text{-}1)$ represents the grid voltage sampled in the previous switching interruption, and $u_{\text{g}}(k\text{-}2)$ represents the grid voltage sampled before $u_{\text{g}}(k\text{-}1)$. Besides, k_1 and k_2 are two coefficients that need to satisfy $k_1 + k_2 = N$.

C. Limitations of Control Delay Compensation

It is impossible to realize the prediction without static error in actual situation. When the delay cannot be completely eliminated, the full feedforward of PCC voltage under weak grid will still lead to system instability.

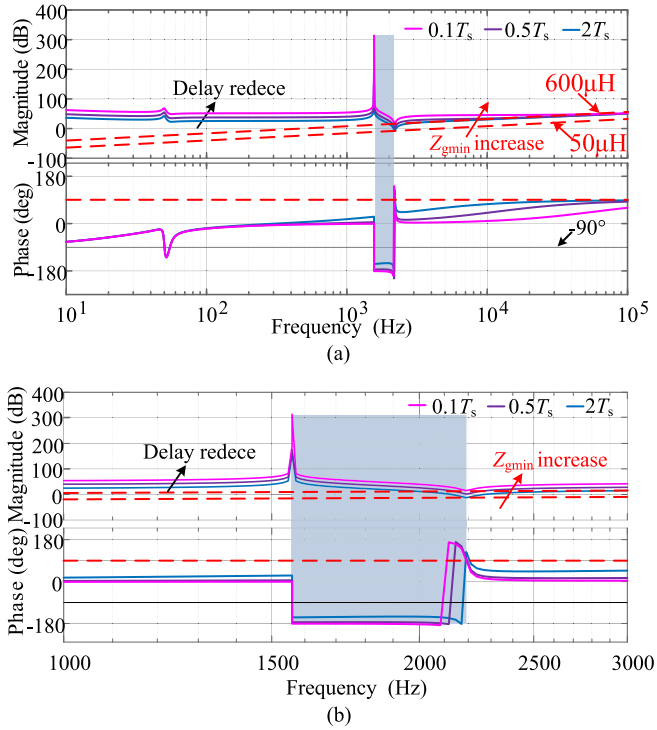

Fig. 9. Bode plots of inverter output impedances with different delay. (a) Overall curves. (b) Detail curves.

TABLE I
MAIN PARAMETERS OF 3 KW PROTOTYPE

Parameters	Value
Rated power P_N	3 kW
DC bus voltage U_{dc}	360 V
Inverter side inductor L_1	1.06 mH
Capacitance C	10 uF
Grid side inductor	1.1 mH
Power grid u_g	220 V/50 Hz
Switching frequency f	18 kHz

Fig. 9 shows the Bode plots of $Z_o(s)$ with $u_{PCC}(s)$ full feedforward when the delay is 2 T_s, 0.5 T_s, and 0.1 T_s, respectively.

According to the parameters in Table I in Section V, it can be calculated that without compensation, L_{gmin} is approximately equal to 50 μH, while after compensation, L_{gmin} is approximately equal to 600 μH. There is no doubt that the critical impedance has increased significantly, but when $Z_g(s)$ exceeds the critical impedance, grid-connected systems will be unstable. Therefore, in order to ensure the stability, additional measures must be added.

IV. Adaptive Adjustment of Virtual Impedance Based on Repetitive Predictive Control

A. Adding Virtual Impedance to Improve System Stability

Based on the above-mentioned analysis, when u_{PCC} is fully feedforward, the instability of system is caused by $Z_g(s)$. And if proportional feedforward is used, the stability margin of the grid-connected system will be increased, but the ability to reject harmonics will be weakened.

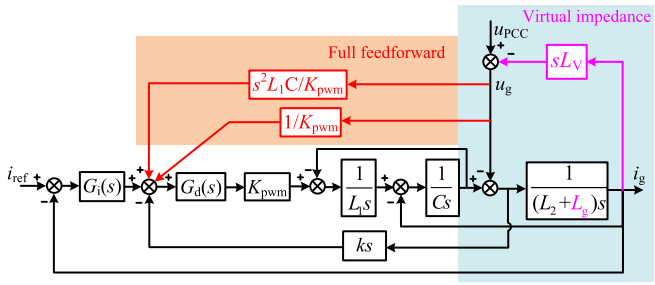

Fig. 10. System control block diagram including virtual impedance and full feedforward of grid voltage.

Therefore, if the weak grid can be changed into a stiff one containing only background harmonics, and the background harmonics can be rejected by full feedforward, then the grid-connected system stability can be ensured and the quality of the injected current can be improved.

Fig. 10 shows a specific implementation scheme, that is, u_{PCC} is subtracted from the voltage of $Z_o(s)$, and then the grid voltage u_g is obtained. $Z_g(s)$ can be regarded as a part of the grid side inductive impedance.

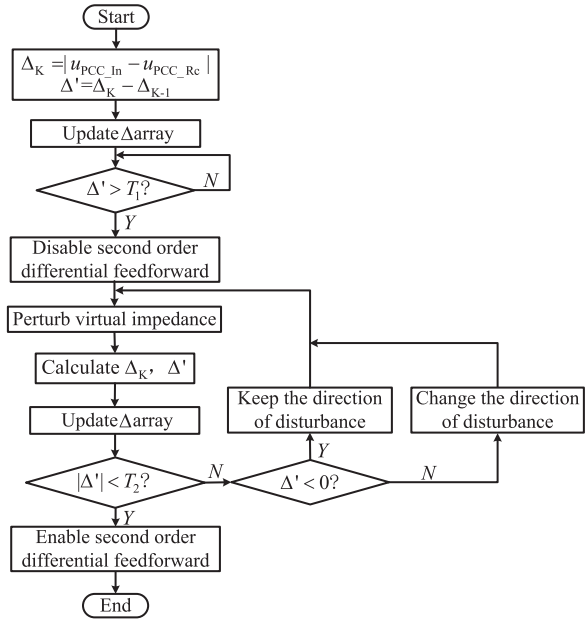

Fig. 11. Flowchart of the proposed adaptive strategy.

B. Strategy of Adaptively Adjusting Virtual Impedance

From the above-mentioned analysis, it can be seen that the system stability and the grid-in current quality are closely related to the grid impedance, and the grid impedance is mainly determined by low power transformers and long distribution lines, and has a time-varying characteristic. The strategy in [18] can accurately calculate the grid impedance by monitoring the amplitude of the inverter voltage and changing the output active and reactive power of the inverter when the voltage amplitude changes. In contrast, we start from another point of view, based on comparing two different methods to predict the difference of u_{PCC}, adaptively modify the value of the virtual impedance online, and determine the optimal virtual impedance with the goal of the optimal grid-in current.

From the above-mentioned analysis, RP hardly amplifies the harmonics of u_g, while other prediction methods, such as NIP, have differential properties that will amplify the harmonics.

And if the virtual impedance is matched with $Z_g(s)$, the stability margin of the grid-connected system is larger, so the influence of i_g on u_{PCC} can be ignored. On the contrary, when $Z_g(s)$ changes greatly, the stability margin decreases, and i_g starts to oscillate resulting in a serious distortion of u_{PCC}.

Therefore, taking $\Delta = |u_{PCC\_NIP} - u_{PCC\_RP}|$ as an indicator, when $Z_g(s)$ changes greatly, Δ will become larger, and if the virtual impedance matches $Z_g(s)$, Δ will acquire the minimum value. Thus, by adaptively modifying the virtual impedance value and finding the minimum Δ value, the virtual impedance can be matched with $Z_g(s)$, thereby stabilizing the grid-connected system and improving the quality of the grid current. The detailed theoretical proof will be given in the next section.

Since the fundamental wave and harmonics of u_{PCC} are periodic, Δ is also periodic. To prevent misjudgment, an array is created to dynamically store Δ. The array size is equal to the number of switching interruptions in one grid cycle. A new Δ is calculated in each interrupt and compared with the earliest one in the array, and then replace the earliest Δ with the latest updated one.

As seen from Fig. 6, when u_g is fully feedforward, if $Z_g(s)$ changes and the difference between $Z_g(s)$ and the virtual impedance exceed Z_{gmin}, the grid-connected system will be instable. In contrast, when adopt proportional feedforward, although the ability to suppress the background harmonics is weakened, the stability margin is relatively large, and the grid-connected system will not lose stability immediately. Therefore, to ensure stability, once the grid impedance is confirmed to have changed and exceeded a critical value, the s^2L_1C/K_{pwm} branch of full feedforward should be disabled first, and then the strategy of adaptively adjusting the virtual impedance begins to work.

The flow chart for adaptively adjusting the virtual impedance based on Δ is shown in Fig. 11. The Δ_K denotes the difference between the two prediction methods at the current moment, and Δ_{K-1} denotes the difference corresponding to the current moment in the previous grid cycle. For example, the difference at the peak of the current grid cycle and the difference at the peak of the previous grid cycle are Δ_K and Δ_{K-1}, respectively.

Δ' represents the difference between Δ_K and Δ_{K-1}. T_1 denotes threshold 1, when Δ' is greater than T_1, it means that the change of $Z_g(s)$ causes large oscillation of u_{PCC}. And T_2 indicates the threshold 2, when the absolute value of Δ' is less than T_2, it means that the virtual impedance has better matched $Z_g(s)$.

The proposed strategy can be divided into two parts, one is the part to confirm $Z_g(s)$ has changed and the other one is to adjust the virtual impedance adaptively. The specific steps are as follows.

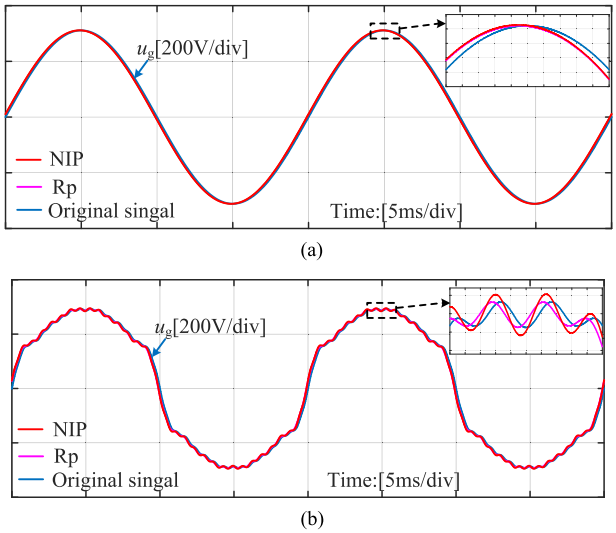

Fig. 12. Comparisons of NIP and RP. (a) $u_g(s)$ undistorted. (b) $u_g(s)$ distorted.

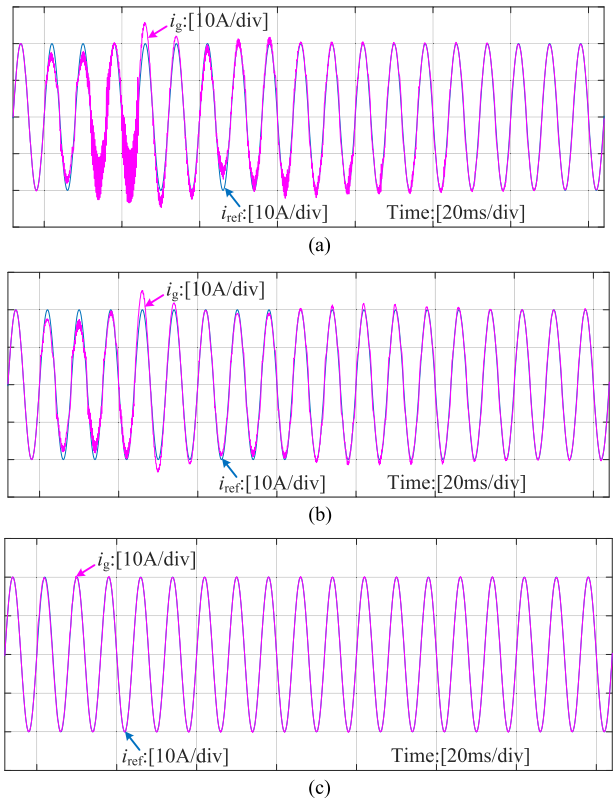

Fig. 13. Virtual impedance adjustment process under different R/X. (a) R/X=0. (b) R/X=1. (c) R/X=2.27.

1) Δ_K is calculated in each switching interrupt and compared with Δ_{K-1} to obtain Δ'.
2) Update the Δ array. The newly obtained Δ replaces the earliest one stored in the array.
3) Judge whether Δ' is greater than T_1. If not, repeat 3), otherwise, disable the s^2L_1C/K_{pwm} branch of full feedforward.

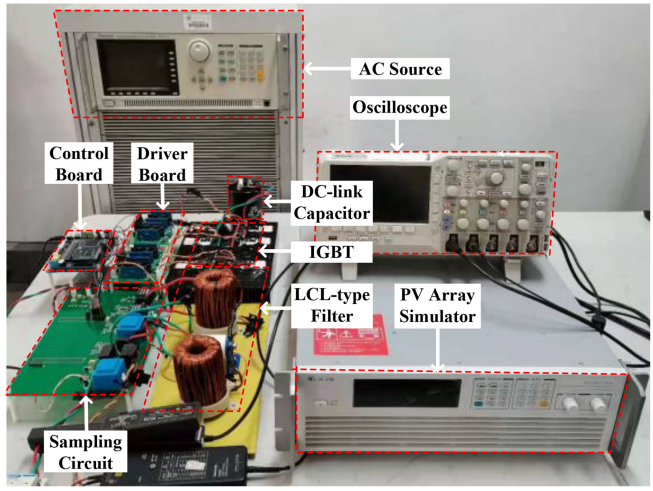

Fig. 14. Photograph of the prototype.

4) Perturb the virtual inductance, and continue to calculate Δ_K and Δ', dynamically update the Δ array.
5) Judge whether $|\Delta$'$|$ is less than T_2, if true, enable the s^2L_1C/K_{pwm} branch of full feedforward and stop adaptively adjusting the virtual impedance. If not, judge whether Δ'<0 is true, if true, keep the direction of the previous virtual impedance perturbation and go to 4), otherwise change the direction and repeat 4).

C. Theoretical Proof of the Proposed Strategy

The most important premise of the proposed strategy is that Δ'>0 holds when $Z_g(s)$ changes. A detailed theoretical proof is given below, which can be divided into two steps.

Step 1: Prove that NIP amplifies the signal more than RP.

When NIP is used to predict u_g, and to reduce the difficulty of proof, (12) can be simplified as

$$u_{out}(k) = u_{in}(k) + k(u_{in}(k) - u_{in}(k-1)) \tag{13}$$

where k represents the predicted number of T_s. Equation (14) can be obtained when (13) divide both sides by T_s

$$\frac{u_{out}(k)}{T_s} = \frac{u_{in}(k)}{T_s} + \frac{k(u_{in}(k) - u_{in}(k-1))}{T_s}. \tag{14}$$

It is not difficult to see that the second term on the right side of (14) is a backward difference, which indicates that NIP has a differential property.

The relationship between $u_{in}(k)$ and $u_{in}(k\text{-}1)$ are expressed

$$u_{in}(k-1) = u_{in}(k)\, e^{-sT_s}. \tag{15}$$

Thus, (13) can be changed as

$$u_{out}(k) = u_{in}(k)(1 + k - ke^{-sT}). \tag{16}$$

The transfer function of NIP can be expressed as

$$G_{NIP}(s) = 1 + k - ke^{-sT_s}. \tag{17}$$

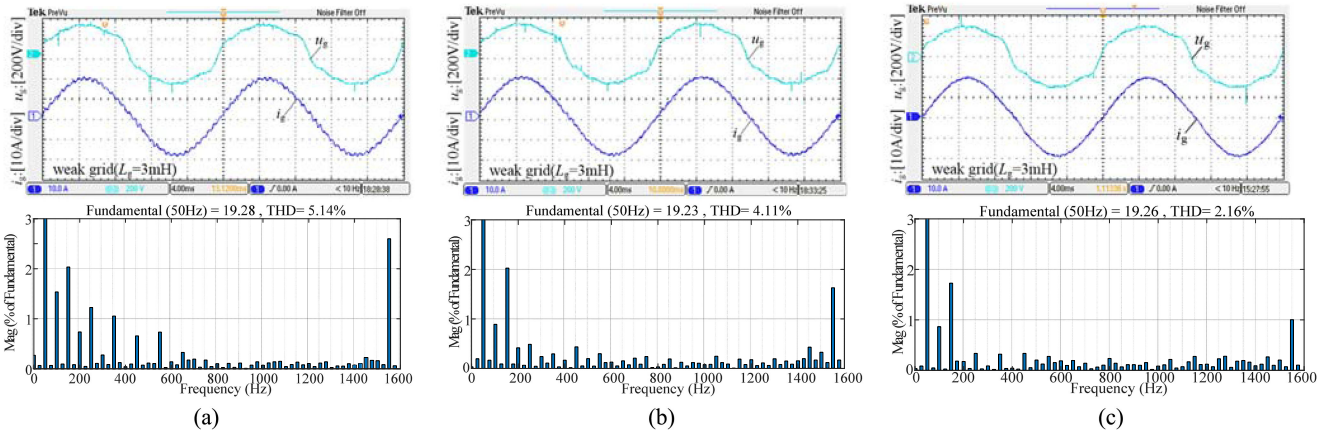

Fig. 15. Comparisons of grid-in currents with different methods. (a) Proportional feedforward. (b) Full feedforward with NIP. (c) Full feedforward with RP.

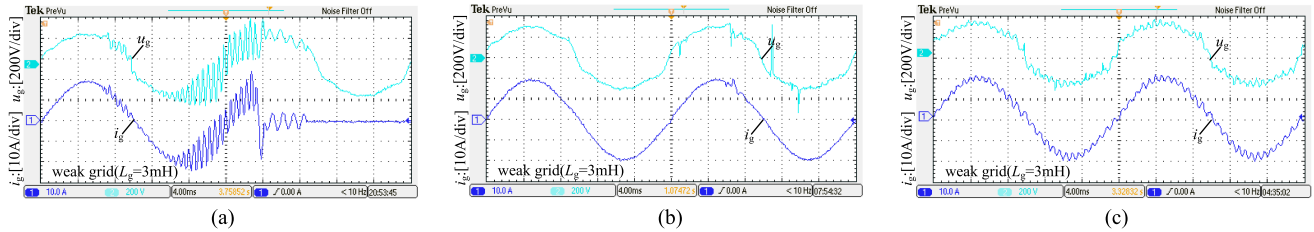

Fig. 16. Process of grid-connected system instability. (a) s^2L_1C/K_{pwm} branch is not prohibited. (b) s^2L_1C/K_{pwm} branch is prohibited. (c) Final waveform with proportional feedforward.

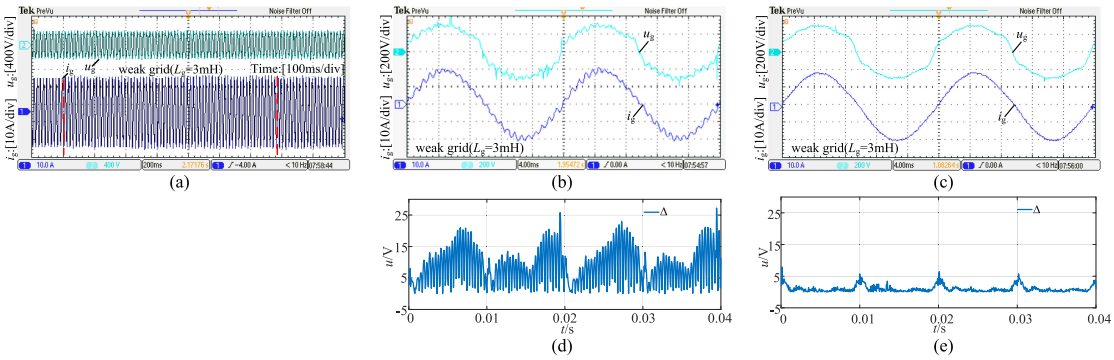

Fig. 17. Proposed strategy subjected to a sudden increase of $Z_g(s)$. (a) Whole process. (b) Adjustment is not over yet. (c) Adjustment is finished. (d) Δ_K when the adjustment is not over yet. (e) Δ_K when the adjustment is finished.

For the convenience of comparison, the transfer function of RP represented by (11) can be changed as

$$G_{\mathrm{RP}}(s)=\frac{1-Qe^{-sNT_s}+me^{-s(N-k)T_s}}{1-Qe^{-sNT_s}+me^{-sNT_s}}. \tag{18}$$

Defining $G_\Delta(s)=G_{\mathrm{NIP}}(s)$-$G_{\mathrm{RP}}(s)$, and the detailed expression of $G_\Delta(s)$ can be obtained

$$G_\Delta(s)=G_{\mathrm{IN}}(s)-G_{\mathrm{RP}}(s)$$

$$=\frac{(1-e^{-sT})(k+km-kQ)+me^{-s(N-k)T}(e^{kT}-1)}{1-Qe^{-sNT}+me^{-sNT}}. \tag{19}$$

Based on the values of k, m, and Q, it can be confirmed that $G_\Delta(s)>0$, which can prove that the amplification of NIP on signal is greater than RP.

Step 2: On the basis of step 1, next to prove that $\Delta'>0$ holds when $Z_g(s)$ changes.

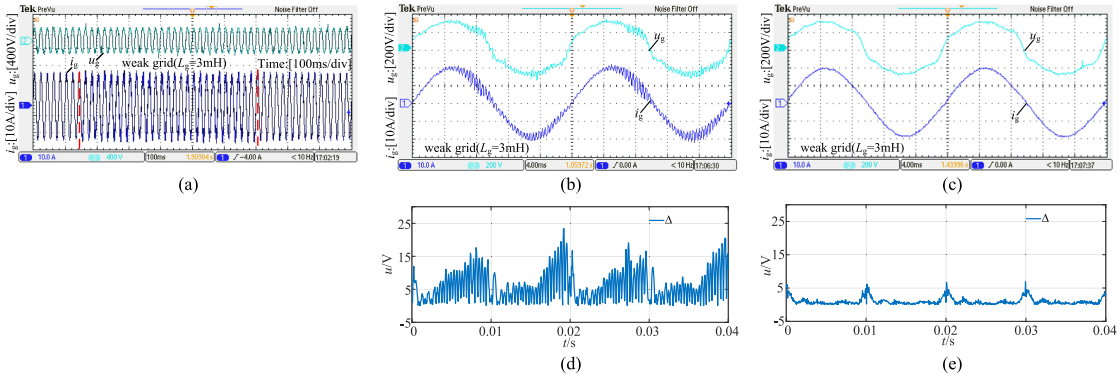

Fig. 18. Proposed strategy subjected to a sudden decrease of $Z_g(s)$. (a) Whole process. (b) Adjustment is not over yet. (c) Adjustment is finished. (d) Δ_K when the adjustment is not over yet. (e) Δ_K when the adjustment is finished.

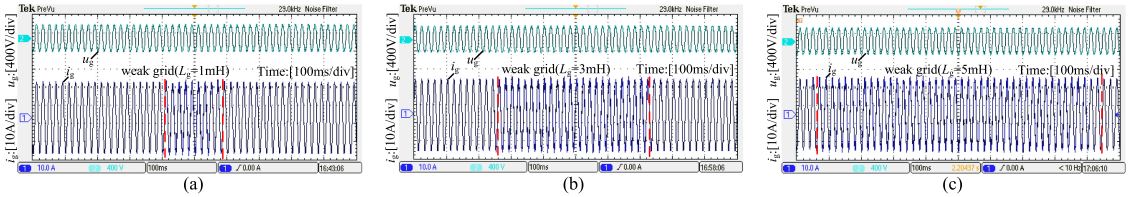

Fig. 19 Waveforms of adjustment process with different SCRs. (a) SCR=51. (b) SCR=17. (c) SCR=10.

Assume that a harmonic voltage in the PCC voltage can be expressed as

$$f_n = A\sin(n\omega t + \varphi). \tag{20}$$

After the changes of $Z_g(s)$, the harmonic expression can be changed as

$$f_n{}' = A_1\sin(n\omega t + \varphi). \tag{21}$$

Thus, the Δ' can be expressed as

$$G_\Delta(s)|f_1| - G_\Delta(s)|f| > 0. \tag{22}$$

The equivalent transformation of (23) can be expressed as

$$G_\Delta(s)(A_1 - A)|\sin(n\omega t + \varphi)| > 0. \tag{23}$$

According to the above analysis, $G_\Delta(s)>0$ is valid. And because once the virtual impedance is not matched with $Z_g(s)$, the injected current will start to oscillate. Due to this current flows through Z_{L2} and Z_g, the voltage at PCC start to oscillate similarly. Thus, the harmonics voltages are increasing, and A_1-$A>0$ is also true.

For a certain harmonic, $|\sin(n\omega+\varphi)|$ contains only two points equal to zero in a cycle, and the rest are greater than zero. Due to u_g contains both fundamental and multiple harmonics, thus the probability of them being zero at the same time is negligible.

V. Verification

A. Simulation

The two prediction methods are validated first based on MATLAB. The working conditions are divided into two cases: 1) u_g contains fundamental voltage only; 2) u_g distorted by 3th, 5th, 7th, 9th, 11th, and 31th harmonics. The magnitudes of harmonics with respect to the fundamental voltage are 10%, 7%, 5%, 3%, 2%, and 1%, respectively.

When u_g is not distorted, both NIP and RP can achieve the purpose of prediction well in Fig. 12(a). On the contrary, if u_g is distorted seriously, NIP will significantly amplify the background harmonics. In contrast, RP hardly changes the background harmonics in Fig. 12(b). It shows that the prediction of RP is much better than NIP under a weak grid.

The adjustments of virtual impedance regulation when the grid impedance contains resistance are shown in Fig. 13. Clearly, the proposed strategy can find the appropriate virtual resistance when the grid impedance changes abruptly at different *R/X* to ensure the quality of the grid-in current.

B. Experiments

A prototype of a 3-kW single-phase grid-connected inverter with an *LCL*-filter is built and tested. The parameters are shown in Table I, and the photo of the inverter is given in Fig. 14.

To get an accurate evaluation of the proposed solution, a programmable ac source (Chroma 61151) is used to simulate the grid voltage distorted by harmonics, and the composition and magnitude of harmonics are consistent with the simulation.

The waveforms and the total harmonic distortion (THD) with different methods are given in Fig. 15, while $Z_g(s)$ does not exist. After employing the proposed full feedforward strategy and using RP to compensate for the delay, the harmonic-rejection-ability of the grid-connected inverter is greatly enhanced under the stiff grid. The measured current THD is the smallest and only 2.16%. By contrast, with the use of proportional feedforward and full feedforward with NIP, the THDs are 5.14% and 4.11%, respectively.

If $Z_g(s)$ is non-negligible and a sudden change occurs, the s^2L_1C/K_{pwm} branch should be prohibited immediately, otherwise grid-connected system will be unstable. After prohibiting, i_g will not immediately start to oscillate, but the grid-connected system stability margin is low, and i_g will gradually oscillate over a period of time. The above process is shown in Fig. 16.

Thus, if a sudden change of $Z_g(s)$ occurs, it is necessary to enable the virtual impedance adaptive adjustment strategy to keep grid-connected systems stable. In the experiment, T_1 and T_2 are set as 5%, 2.5% of the fundamental of u_g, respectively.

Figs. 17 and 18 show the waveforms when the grid impedance increases and decreases abruptly, respectively. Among them, Figs. 17(a) and 18(a) give the whole dynamic regulation process. Figs. 17(b) and 18(b) show the current waveforms when the optimal virtual impedances have not yet been found, and there is a significant oscillation in the grid-in current. In contrast, Figs. 17(c) and 18(c) display the steady-state waveforms of the grid-in current after finding the optimal virtual impedance. The quality of the grid-in current is satisfactory with the proposed strategy, despite the fact that the grid impedance cannot be neglected and the grid voltage has serious distortions. Figs. 17(c) and 18(c) give the difference between the two prediction methods in predicting u_{PCC} when the virtual impedance adjustment is not yet completed. As a comparison, Figs. 17(e) and 18(e) show the difference between the two prediction methods in predicting u_{PCC} after the virtual impedance adjustment is completed. It can be seen that there is a significant oscillation in u_{PCC} when the virtual impedance adjustment is not completed, resulting in a larger oscillation in the difference between the two prediction methods. In contrast, when the virtual impedance adjustment is completed, the difference between the two methods predictions is smaller. The above-mentioned experimental results demonstrate the effectiveness of the proposed strategy.

To further verify the effectiveness of the proposed strategy, experiments were conducted with different short-circuit capacity ratios (SCR) of the system when the grid impedance decrease suddenly. The experimental results are shown in Fig. 19. It can be found that as the SCR decreases, i.e., the grid impedance increases, the time for the proposed strategy to regulate the virtual impedance increases, but eventually a suitable virtual impedance can still be found to stabilize the system and ensure the grid-in current quality.

VI. Conclusion

An adaptive strategy based on repetitive control for improving adaptability of *LCL* grid-connected inverters under weak grid is investigated in this article. The major outcomes include the following.

1) The full feedforward strategy of grid voltage ug based on the differential feedback of grid side inductor voltage active damping is derived, which reduces the complexity of the existing full feedforward, and the relationship between grid voltage full feedforward and the output impedance of the grid-connected inverter is revealed.
2) The influence of the control delay on full feedforward strategy is analyzed, and the delay is compensated by the repetitive control. It is proved that a grid-connected system is more sensitive to the delay when grid voltage is fully feedforward. The stability of the grid-connected inverter cannot be guaranteed only by compensating for the delay under a weak grid, and the virtual impedance branch is added.
3) Based on the difference between RP and Newton interpolation prediction of voltage at PCC, the proposed strategy adaptively modifies the virtual impedance online, which can ensure the stability of the grid-connected system when the grid impedance changes, improving the adaptability of the grid-connected inverters to the weak grid.

References

[1] E. Rodriguez, F. D. Freijedo, J. C. Vasquez, and J. M. Guerrero, "Analysis and comparison of notch filter and capacitor voltage feedforward active damping techniques for LCL grid-connected converters," *IEEE Trans. Power Electron.*, vol. 34, no. 4, pp. 3958–3972, Apr. 2020.

[2] Z. Miao, W. Yao, and Z. Lu, "Single-cycle-lag compensator-based active damping for digitally controlled LCL/LLCL-type grid-connected inverters," *IEEE Trans. Ind. Electron.*, vol. 67, no. 3, pp. 1980–1990, Mar. 2020.

[3] A. Adib and B. Mirafzal, "Virtual inductance for stable operation of grid-interactive voltage source inverters," *IEEE Trans. Power Electron.*, vol. 66, no. 8, pp. 6002–6011, Aug. 2019.

[4] Y. Guan, Y. Wang, Y. Xie, Y. Liang, A. Lin, and X. Wang, "The dual-current control strategy of grid-connected inverter with LCL filter," *IEEE Trans. Power Electron.*, vol. 34, no. 6, pp. 5940–5952, Jun. 2019.

[5] K. Zhu, P. Sun, L. Zhou, X. Du, and Q. Luo, "Frequency-division virtual impedance shaping control method for grid-connected inverters in a weak and distorted grid," *IEEE Trans. Power Electron.*, vol. 35, no. 8, pp. 8116–8129, Aug. 2020.

[6] H. Wang, X. Ruan, S. Liu, and C. Tse, "Full feedforward of grid voltage for grid-connected inverter with LCL filter to suppress current distortion due to grid voltage harmonics," *IEEE Trans. Power Electron.*, vol. 15, no. 12, pp. 3119–3127, Dec. 2010.

[7] W. Li, X. Ruan, D. Pan, and X. Wang, "Full-feedforward schemes of grid voltages for a three-phase LCL-type grid-connected inverter," *IEEE Trans. Power Electron.*, vol. 60, no. 6, pp. 2237–2250, Jun. 2013.

[8] D. Zhu, S. Zhou, X. Zou, and Y. Kang, "Improved design of PLL controller for LCL-type grid-connected converter in weak grid," *IEEE Trans. Power Electron.*, vol. 35, no. 5, pp. 4715–4727, May 2020.

[9] D. Yang, X. Ruan, and H. Wu, "Impedance shaping of the grid-connected inverter with LCL filter to improve its adaptability to the weak grid condition," *IEEE Trans. Power Electron.*, vol. 29, no. 11, pp. 5795–5805, Nov. 2014.

[10] Z. Lin, X. Ruan, L. Wu, H. Zhang, and W. Li, "Multi resonant component-based grid-voltage-weighted feedforward scheme for grid-connected inverter to suppress the injected grid current harmonics under weak grid," *IEEE Trans. Power Electron.*, vol. 35, no. 9, pp. 9784–9793, Sep. 2020.

[11] M. Davari and Y. Mohamed, "Robust vector control of a very weak-grid-connected voltage-source converter considering the phase-locked loop dynamics," *IEEE Trans. Power Electron.*, vol. 32, no. 2, pp. 977–994, Feb. 2017.

[12] L. Zhou *et al.*, "Inverter-current-feedback resonance-suppression method for LCL-type DG system to reduce resonance-frequency offset and grid-inductance effect," *IEEE Trans. Ind. Electron.*, vol. 65, no. 9, pp. 7036–7048, Sep. 2018.

[13] R. Luhtala, H. Alenius, T. Messo, and T. Roinila, "Online frequency response measurements of grid-connected systems in presence of grid harmonics and unbalance," *IEEE Trans. Power Electron.*, vol. 35, no. 4, pp. 3343–3347, Apr. 2020.

[14] P. Garcia, M. Sumner, A. Navarro-Rodriguez, J. M. Guerrero, and J. Garcia, "Observer-based pulsed signal injection for grid impedance estimation in three-phase systems," *IEEE Trans. Ind. Electron.*, vol. 65, no. 10, pp. 7888–7899,Oct. 2018.

[15] T. Roinila, T. Messo, and E. Santi, "MIMO-identification techniques for rapid impedance-based stability assessment of three-phase systems in DQ domain," *IEEE Trans. Power Electron.*, vol. 33, no. 5, pp. 4015–4022, May 2018.
[16] A. V. Timbus, P. Rodriguez, R. Teodorescu, and M. Ciobotaru, "Line impedance estimation using active and reactive power variation," in *Proc. IEEE Power Electron. Spec. Conf.*, 2007, pp. 1273–1279.
[17] N. Mohammed, M. Ciobotaru, and G. Town, "An improved grid impedance estimation technique under unbalanced voltage conditions," in *Proc. IEEE PES Innov. Smart Grid Technol. Eur.*, 2019, pp. 1–5.
[18] N. Mohammed, T. Kerekes, and M. Ciobotaru, "An online event-based grid impedance estimation technique using grid-connected inverters," *IEEE Trans. Power Electron.*, vol. 36, no. 5, pp. 6106–6117, May 2021.
[19] H. Wang, X. Ruan, S. Liu, and C. Tse, "Full feedforward of grid voltage for grid-connected inverter with LCL filter to suppress current distortion due to grid voltage harmonics," *IEEE Trans. Power Electron.*, vol. 25, no. 12, pp. 3119–3127, Dec. 2010.
[20] M. Lu, X. Wang, P. Log, F. Blaabjerg, and T. Dragiceiv, "Graphical evaluation of time-delay compensation techniques for digitally controlled converters," *IEEE Trans. Power Electron.*, vol. 33, no. 3, pp. 2601–2614, Mar. 2017.
[21] D. Yang, X. Ruan, and H. Wu, "A real-time computation method with dual sampling mode to improve the current control performance of the LCL-type grid-connected inverter," *IEEE Trans. Ind. Electron.*, vol. 62, no. 7, pp. 4563–4572, Jul. 2015.
[22] D. Guindon, D. Shpak, and A. Antoniou, "Design methodology for nearly linear-phase recursive digital filters by constrained optimization," *IEEE Trans. Circuits Sys. I Reg. Papers*, vol. 57, no. 7, pp. 1719–1731, Jul. 2010.
[23] S. Eren, M. Pahlevaninezhad, A. Bakhshai, and P. K. Jain, "Composite nonlinear feedback control and stability analysis of a grid-connected voltage source inverter with LCL filter," *IEEE Trans. Ind. Electron.*, vol. 60, no. 11, pp. 5059–5074, Nov. 2013.
[24] L. Zhou *et al.*, "Harmonic voltage distortion damping method for parallel-connected LCL-type inverters in islanded operation," *IEEE Trans. Ind. Electron.*, vol. 66, no. 11, pp. 9032–9044, Nov. 2019.
[25] C. Xie, D. Liu, K. Li, J. Zou, and J. M. Guerrero, "Passivity-based design of repetitive controller for LCL-type grid-connected inverter suitable for microgrid applications," *IEEE Trans. Power Electron.*, vol. 36, no. 2, pp. 2420–26431, Feb. 2021.
[26] J. S. H. Tsai, T. J. Tsai, and S. Guo, "Observer with evolutionary-programming-based optimal digital tracker for analog neutral multiple time-delay systems," *Appl. Math. Comput.*, vol. 188, no. 1, pp. 1001–1015, May 2007.

Mingming Li was born in Jiangsu Province, China. He received the B.S. degree in automation engineering from Hohai University, Nanjing, China, in 2013. He is currently working toward the Ph.D. degree in electrical engineering with Southeast University, Nanjing, China.

His current research interests include grid-connected inverters' control and system stability analysis.

Huafeng Xiao (Senior Member, IEEE) was born in Hubei Province, China. He received the B.S., M. S., and Ph.D. degrees in electrical engineering from the Nanjing University of Aeronautics and Astronautics, Nanjing, China, in 2004, 2007, and 2010, respectively.

He joined the Faculty of Power Electronics in 2011, and is currently a Professor with the College of Electrical Engineering, Southeast University, Nanjing, China. From 2015 to 2016, he was a Postdoctoral Fellow with the Department of Electrical and Computer Engineering, Ryerson University, Toronto, ON, Canada. From August 2016 to 2017, he was a Postdoctoral Fellow with the Department of Electrical and Computer Engineering, McGill University, Montreal, QC, Canada. He has authored more than 100 technical papers in journals and conference proceedings, and held 36 China patents and 1 U.S. patent, and authored two books as well. His research interests include transformerless photovoltaic power systems, and high frequency soft-switching conversions.

Ming Cheng (Fellow, IEEE) received the B.Sc. and M.Sc. degrees from the Department of Electrical Engineering, Southeast University, Nanjing, China, in 1982 and 1987, respectively, and the Ph.D. degree from the Department of Electrical and Electronic Engineering, The University of Hong Kong, Hong Kong, in 2001, all in electrical engineering.

Since 1987, he has been with Southeast University, where he is currently a Chair Professor with the School of Electrical Engineering and the Director of the Research Center for Wind Power Generation. From January to April 2011, he was a Visiting Professor with Wisconsin Electric Machine and Power Electronics Consortium, University of Wisconsin, Madison, Madison, WI, USA. He has authored or coauthored more than 360 technical papers and 4 books and is the holder of 100 patents in these areas. His teaching and research interests include electrical machines, motor drives for electric vehicles, and renewable energy generation.

Dr. Cheng is a Fellow of the Institution of Engineering and Technology. He has served as the Chair and organizing committee member for many international conferences. He is a Distinguished Lecturer of the IEEE Industry Applications Society in 2015 and 2016.